Electronic Journal of Structural Engineering

Original Article

Cite this: DOI:10.56748/ejse.24776

Received Date: 5 March 2025
Accepted Date:29 October 2025

1443-9255
https://ejsei.com/ejse

Assessment of fiber-reinforced rubberized recycled aggregate concrete properties by optimal regression frameworks

Liqing Hao [a], Yuexiang Li [a*], Dongfang Zhang [a]

[a] College of Civil Engineering and Architecture, Hebei University of Engineering Science, Shijiazhuang 050091, Hebei, China
*Corresponding author: liyuexiang026@126.com

Abstract

The rapid increase in construction and demolition (C&D) waste, as well as discarded tires, presents a significant environmental challenge globally. To address this issue, the current study develops and assesses advanced regression-based machine learning models to predict the flexural strength (fs) of fiber-reinforced rubberized recycled aggregate concrete (FRRAC). Two innovative hybrid models, LSSVR(A) and LSSVR(C), are introduced by combining Least Squares Support Vector Regression (LSSVR) with the Artificial Rabbit Optimization Algorithm (AROA) and Chimp Optimization Algorithm (ChOA), respectively, to optimize hyperparameters. A comprehensive dataset of 102 experimental samples was used, with 75% allocated for training and 25% for testing. The performance of both hybrid models was evaluated through multiple statistical measures. Results showed that LSSVR(A) delivered better prediction accuracy (R^2 = 0.9895 for training and 0.9825 for testing) and lower uncertainty than LSSVR(C). These findings demonstrate the effectiveness of combining metaheuristic optimization with regression-based learning for accurately predicting FRRAC properties. The proposed models offer a dependable computational tool for designing sustainable concrete mixes that optimize strength, cost efficiency, and environmental impact.

Keywords

Concrete, Recycled aggregate, Fiber, Crumb rubber, LSSVR

1. Introduction

The amount of waste produced by construction and demolition (CD) is increasing rapidly, positioning it as one of the primary resources of rubbish for mankind. This CD makes up thirty and forty percent of the garbage that is produced annually in the world (Hossain et al., 2019). Vehicle tyre debris is an additional potential waste source for construction. Rubber's nonbiodegradability, flammability, and chemical makeup make it a major threat to both environmental and human safeties. Approximately 3 billion tyres are produced commercially each year in the globe to meet the needs of the economy, and roughly the identical number are approaching the end of their useful lives (Grammelis et al., 2021). The number of discarded tyres will surpass that of current tyres by 2030. Using crumb rubber (CR) from discarded tyres as a material has been shown in certain experiments to reduce carbon dioxide emissions by as much as 0.41%, depending on the substitution amount of CR (Mhaya et al., 2020). In order to produce an environmentally friendly green construction, scholars are working to reuse these sorts of recyclable parts or using alternative nanoparticles for ecological cleaning and the generation of green energy.

Many studies have been conducted on recycled coarse aggregate (RCA), which is substituted with different ratios of natural coarse aggregate (NCA)(Hossain et al., 2019; Shafighfard et al., 2022). Accessibility, average weight, strength in compression, modulus of elasticity, and water absorption (due to the glue connecting the RCA layer) were among the areas where RAC performed worse than NAC (Revilla-Cuesta et al., 2022a). Revilla-Cuesta (Revilla-Cuesta et al., 2022b) states that the elasticity modulus of RAC is 2.5 times that of the toughened density. Due to the material's raised porosity and lower density, the usage of RCA reduced the UPV (Espinosa et al., 2023). Up to 100% of RCA might be absorbed, according to many investigations (Guo et al., 2014; Henry et al., 2012; Li et al., 2016; Liu et al., 2015; Su, 2015; Xie et al., 2018, 2015). However, when 25–50% RCA was utilised, there was a little but discernible drop in the mechanical properties of concrete. As much as half of the natural fine aggregates (NFA) in the mixture may be substituted with the most popular kind of rubber aggregate, known as the CR (Shahjalal et al., 2019; Zhang et al., 2024). Rubberized concrete (RuC) has many benefits, including enhanced impact resistance, increased damping characteristics, developed ductility and strength, increased resistance to cracking and spalling, increased capacity to absorb sound and thermal insulation, and resistance to the freezing and thawing procedure, despite the fact that its low resilience is an important disadvantage. Moreover, increasing the CR content causes the fracture trend to shift from shearing cracking to flexural cracking, and (RuC) has a more progressive failure structure (Bandarage and Sadeghian, 2020; Moustafa and ElGawady, 2017). Investigations on the combined effects of RCA and CR (Li et al., 2016; Liu et al., 2015), as well as RCA, CR, and other fibres (Guo et al., 2014; Xie et al., 2018, 2015), on concrete have recently been carried out. When comparing the rubberized RAC (RRAC) mixture to the regular mixture, the sintest Marie (Marie, 2017) saw a decrease in the droop rate. In particular, the slump grade decreased by almost 42% when RCA and CR made up 20% of the combination. The results of the Hossain et al. research (Hossain et al., 2019) shown a 76.4% reduction in slump levels for the fiber-reinforced RAC (FRRAC) mixture. This decline was seen for a variety of PP fibre percentages (0–2%), CR percentages (0–10%), and RCA percentages (0–30%). Study by Ahmed et al. (Ahmed et al., 2019) demonstrated that the resilience of compression of FRRAC may be up to 31% more than that of its fiber-free counterpart. The strength of flexion of RRAC is determined by the size of the CR particle, as per earlier studies conducted in 2016 (Li et al., 2016) and 2015 (Su, 2015). The flexural strength of RRAC decreased significantly, but Feng et al. (Liu et al., 2015) managed to raise it to more than 4.5 MPa by lowering the CR content to 20%. Comparatively, the flexural strengths of FRRAC mixtures with fibre additions were much greater (Piri et al., 2023)

1.1 Machine learning applications

Over the course of the last several years, there has been an increase in the application of machine learning (ML) techniques for the purpose of predicting structural systems (Chen et al., 2022; Çiftçioğlu et al., 2025; Hemmatian et al., 2023; Shafighfard et al., 2025). The use of ML approaches (Wang et al., 2025; Zhang et al., 2025) which could predict the impact of fibre, RCA, or CR on mechanical qualities has been the subject of a significant amount of research (El-Khoja et al., 2018). In a significant number of these studies initiatives, the goal was to make predictions about compressive strengths. A limited number of studies (Gupta et al., 2019; Huang et al., 2021; Kazemi et al., 2025; Miladirad et al., 2021; Zhang et al., 2021) were conducted on the following characteristics: breaking tensile strength, flexural strength, unit weight, elasticity modulus, flow table, and shear strength. Four ML techniques were utilised by de-Prado-Gil et al. (de-Prado-Gil et al., 2022) in order to make a prediction about the splitting tensile strength of Self-Compacting RAC ($SRAC$) according to 381 data samples. With a R^2 value of 0.8423, the $XGBoost$ model was shown to have exceeded the performance of the other models presented in the study. A dataset that had 712 data points was used by Golafshani et al. (Golafshani et al., 2021) in order to make a prediction about the compression strength of concrete that was manufactured of rubber (RuC). $MGEP$, which stands for multi-gene expression programming, was employed in conjunction with two different ML architectures, such as the $M5P$ model tree.

Table 1. Overview of earlier ML-based concrete studies

Reference	Output (Target)	Typical Inputs (as reported/typical)	ML model(s)	Dataset size	Metrics & best reported accuracy
de-Prado-Gil et al.	Splitting tensile strength (SCC)	Mix features incl. w/c, aggregate & fiber characteristics	4 ML techniques; best model reported	381	R = 0.8423 (best model)
Golafshani et al.	Compressive strength (rubberized concrete)	Mix features incl. w/c, aggregate & fiber characteristics	MGEP + model-tree architectures	712	Highest accuracy among compared models (values reported in study)
Avijit Pal et al.	Compressive strength	w/c, aggregate properties, fiber content (key parameters across studies)	13 ML models benchmarked; CatBoost best	905	CatBoost showed highest accuracy among 13 models
Çakıroğlu et al.	Compressive & tensile strength	w/c, aggregate properties, fiber content	CatBoost (dominant)	451	CatBoost confirmed as top performer
Alabduljabbar et al.	Split tensile strength	w/c, aggregate properties, fiber content	GEP	257	R = 0.983 (excellent)
Alarfaj et al.	Split tensile strength	w/c, aggregate properties, fiber content	Deep Neural Networks	—	R^2 = 0.94 (DNN superior)
Avijit Pal et al.	Slump	w/c, aggregate properties, fiber content	XGBoost	464	Demonstrated high effectiveness for slump prediction
Zhang et al.	(Various; comparison study)	Mix features	ELM vs. conventional ANNs	—	ELM showed remarkable precision vs. traditional NNs
Huang et al. [25]	Various mechanical properties	Mix features	ANN (Levenberg–Marquardt)	—	Successful predictions across properties
Rahman et al. [35]	Shear strength (FRC frames)	Structural/material features	11 ML techniques; tree-based forecasters superior	—	Tree-based models are superior to others

Utilizing CR levels that range from 2 to 6% is allowed for the discovery of the most effective mix designs for (RuC).

In a study conducted by Zhang et al. (Zhang et al., 2021), it was shown that the extreme machine learning system (EMLS) had remarkable precision in comparison to more conventional neural networks (NN) such as BPNN and SVM. It is possible to employ an ANN framework in conjunction with the Levenberg-Marquardt (LM) approach in the research carried out by Huang et al. (Huang et al., 2021) to predict a variety of mechanical properties of (RuC). Eleven ML techniques were utilised by Rahman et al. (Rahman et al., 2021) in order to assess the strength in shear of fibre reinforced concrete frames. The XGBoost forecasters were shown to be superior to the other methods in terms of their ability to accurately estimate the power. In a separate piece of study, a comprehensive gathering of empirical data was produced. This collection comprised measurements of the flexural strength of FRRAC and consisted of 102 samples obtained from a variety of resources. The evidence includes over 2,200 experimental data points from various studies. For compressive strength prediction, (Pal et al., 2023) evaluated 13 ML models on 905 samples, with CatBoost showing the highest accuracy. Similarly, Celal Çakıroğlu et al., (Cakiroglu et al., 2023a) confirmed CatBoost's dominance using 451 samples for compressive strength and 151 for tensile strength. Regarding split tensile strength, Hisham Alabduljabbar et al. (Alabduljabbar et al., 2024), reported excellent results with Gene Expression Programming (R=0.983) on 257 samples, although Mohammed Alarfaj et al. (Alarfaj et al., 2024), found Deep Neural Networks to be superior (R^2=0.94). Additionally, Avijit Pal et al. (Pal et al., 2024), demonstrated XGBoost's effectiveness in slump prediction with 464 data points. Consistently identified key parameters influencing results include water/cement ratio, aggregate properties, and fiber content Avijit Pal et al., (Pal et al., 2024); Celal Çakıroğlu et al. (Cakiroglu et al., 2023a), . Overall, these studies show that advanced ML frameworks significantly outperform traditional regression methods in assessing FRRAC properties.

1.2 Hybrid LSSVR Models for Predicting Flexural Strength of FRRAC

Construction and demolition (C&D) waste exceeds 10 billion tons yearly, representing 30-40% of waste. Over 1 billion tires are generated annually, creating environmental issues. Both relate to UN SDG 12, which promotes responsible consumption, recycling, and reuse. Recycling C&D as RCA and adding crumb rubber (CR) from waste tires can lower the environmental impact but may weaken the strength. Fiber reinforcement and optimized mixes offer solutions, though modeling their effects is complex. This study develops two hybrid models, LSSVR(A) and LSSVR(C), using Support Vector Regression with Artificial Rabbit Optimization and Chimp Optimization. Based on 102 samples, these models predict the flexural strength of fiber-reinforced rubberized recycled concrete, supporting sustainable design and the circular economy.

Table 2. The statistical values of the introduced dataset

1.3 The novelty of present study

In order to determine which regression-based and machine learning techniques are the most successful in predicting the flexural strength (f_s) of fiber-reinforced rubberized recycled aggregate concrete (FRRAC), the purpose of this study is to evaluate and select the most effective methods. A great number of machine learning techniques that make use of regression-based approaches were created in order to achieve this goal. For the purpose of their creation, a mixture of these tactics was employed. For the purpose of doing this, a subset of 102 samples taken from the existing body of research was utilised to train and evaluate tree models for the purpose of f_s prediction. In the computer study that was demonstrated to be effective, a regression-based technique that is referred to as Least square support vector regression (LSSVR) was utilized. For the purpose of achieving the objective of achieving the desired outcome, this approach was taken into account and used. According to the findings of the study, the hyperparameters of the LSSVR have a substantial impact on both its accuracy and its effectiveness. These hyperparameters may be discovered via the use of metaheuristic optimisation techniques. For this particular aim, the Artificial rabbit optimisation algorithm (AROA) and the Chimp optimisation algorithm (ChOA) have been selected as the two methodologies that have been developed in recent times.

2. Methodology

2.1 Data collection

There were previous empirical studies that studied the link between RCA, CR, and fibre, especially rubberized recycled aggregate concrete (RRAC) or fibre reinforced rubberized recycled aggregate concrete (FRRAC)(Ahmed et al., 2019; Aslani et al., 2018; Bahraq et al., 2022; Cakiroglu et al., 2023b; Hossain et al., 2019; Islam and Shahjalal, 2021; Kazemi et al., 2024; Li et al., 2016; Liu et al., 2015; Marie, 2017; Piri et al., 2023; Qaidi et al., 2021; Shahjalal, 2022; Su, 2015; Xie et al., 2018).

Dataset and scope

The data set used in this study was compiled from prior investigations and employed to forecast the flexural strength (f_s) of FRRAC. In total, 102 samples were analyzed for f_s prediction using LSSVR-based models. The training set and the evaluation set each have their own set of input variables and sets of unique statistical measures, which are shown in Table 2. The variables that were included in the input group were as follows: : $Input_1$ (Water-to-cement ratio), $Input_2$ (NCA fineness modulus), $Input_3$ (NCA amount), $Input_4$ (RCA fineness modulus), $Input_5$ (RCA absorption capacity), $Input_6$ (RCA amount), $Input_7$ (RCA substitution level), $Input_8$ (NFA fineness modulus), $Input_9$ (NFA amount), $Input_{10}$ (CR fineness modulus), $Input_{11}$ (CR amount), $Input_{12}$ (CR replacement level), $Input_{13}$ and $Input_{14}$ (Fiber amount), $Input_{15}$ (Kind of fiber (No fiber)), $Input_{16}$ (Kind of fiber (PP)), $Input_{17}$ (Kind of fiber ($Steel$)), $Input_{18}$ (Kind of fiber ($Steel\ Tire\ Wires$)), and $Input_{19}$ (Age of concrete).

Category	Phase	Indices					
		Minimum	Maximum	Standard deviation	Variance	Skewness	Range
$I_1\ (Unit: -)$	Train	0.31	0.45	0.048	0.002	-0.982	0.14
	Test	0.34	0.45	0.042	0.002	-0.110	0.11
$I_2\ (Unit: -)$	Train	0	6.73	3.315	11.135	0.0282	6.73
	Test	0	6.73	3.073	9.839	-0.819	6.73
$I_3\ (Unit: kg/m^3)$	Train	0	1443	430.616	187869.76	0.4196	1443
	Test	0	990.2	365.827	139405.98	-0.512	990.2
$I_4\ (Unit: -)$	Train	0	6.73	2.110	4.510	-2.422	6.73
	Test	0	6.73	2.126	4.710	-2.480	6.73
$I_5\ (Unit: \%)$	Train	0	8.02	1.633	2.703	1.1666	8.02
	Test	0	8.02	1.818	3.443	1.072	8.02
$I_6\ (Unit: kg/m^3)$	Train	0	1340	467.020	220977.98	0.3873	1340
	Test	0	1340	387.806	156659.7	0.945	1340
$I_7\ (Unit: \%)$	Train	0	100	36.454	1346.377	-0.014	100
	Test	0	100	33.600	1176.0	0.619	100
$I_8\ (Unit: -)$	Train	1.47	2.8	0.492	0.245	-1.074	1.33
	Test	1.47	2.8	0.425	0.189	-1.351	1.33
$I_9\ (Unit: kg/m^3)$	Train	336	874	154.221	24096.98	-0.069	538
	Test	504	874	107.974	12144.08	0.446	370
$I_{10}\ (Unit: -)$	Train	0	3.49	1.130	1.295	-1.162	3.49
	Test	0	3.49	1.416	2.088	0.165	3.49
$I_{11}\ (Unit: kg/m^3)$	Train	0	475	122.127	15111.19	2.0526	475
	Test	0	475	114.344	13619.3	3.154	475
$I_{12}\ (Unit: \%)$	Train	0	50	13.614	187.779	0.9144	50
	Test	0	50	12.406	160.323	2.211	50
$I_{13}\ (Unit: kg/m^3)$	Train	0	78	12.772	165.267	5.2077	78
	Test	0	78	24.792	640.247	2.237	78
$I_{14}\ (Unit: \%)$	Train	0	2	0.485	0.238	1.9113	2
	Test	0	2	0.668	0.465	1.051	2
$I_{15}\ (Unit: -)$	Train	0	1	0.497	0.250	-0.24	1
	Test	0	1	0.500	0.260	0.085	1
$I_{16}\ (Unit: -)$	Train	0	1	0.406	0.167	1.4692	1
	Test	0	1	0.466	0.227	0.822	1
$I_{17}\ (Unit: -)$	Train	0	1	0.159	0.026	6.0795	1
	Test	0	1	0.325	0.110	2.491	1
$I_{18}\ (Unit: -)$	Train	0	1	0.406	0.167	1.4692	1
	Test	0	1	0.271	0.077	3.298	1
$I_{19}\ (Unit: Days\ )$	Train	28	180	36.685	1363.516	2.5437	152
	Test	28	180	38.866	1573.493	1.905	152
$Target\ (Mpa\ )$	Train	2.5	11.72	1.936	3.798	1.4356	9.22
	Test	3.2	11.49	2.083	4.520	1.923	8.29

Data partitioning and statistical consistency

To facilitate model development and evaluation, the database was divided into learning (training) and evaluation (testing) subsets. Seventy-five percent (77 samples) were allocated for training, with the remaining twenty-five percent (25%) for testing. After splitting, a statistically significant correlation between the variables in the training and testing groups was observed, demonstrating consistency across the partitions. Each subset maintained its own input variables and related statistical descriptors, as summarized in Table 2.

Encoding and data preparation

The type of fiber was treated as a categorical parameter and encoded accordingly (No fiber, PP, Steel, Steel Tire Wires). When any input was missing, its value was assigned based on standard criteria for structural concrete. For reference, Fig. 1 shows the distribution of input features for the compressive strength dataset.

One kind of statistical analysis known as Kendall analysis, also known as Kendall's tau, is employed in order to ascertain the level of correlation that exists between two ranking criteria. It evaluates the degree to which a monotonic function is able to properly represent the link between the variables. In contrast to Pearson's correlation, that studies linear relationships, Kendall's tau investigates the ordinal link between the two variables, focusing on the ranks rather than the exact values. In the range of potential values for the coefficient, there is a range from -1 to +1. The presence of positive numbers indicates that there is a positive association between the two parameters. This suggests that an increase in one variable often results in an increase in another variable. The presence of negative numbers is indicative of a negative relationship, that indicates that as the value of one parameter grows, the value of the other variable then starts to decline. The Kendall analysis is shown over here in Fig 2. There are times when the variables have low correlated values that are significant enough to demand attention. When developing models utilizing these inputs, it is essential to obtain the highest possible degree of precision in order to create accurate models. As can be seen in Fig 2, the Kendall coefficient between $In6/In7$, and $In12/In11$ both are 0.9, which indicates that there is a strong positive link between the two. In addition, the Kendall coefficient, which has a value of -0.9, demonstrates the most significant negative connection among $In3/In7$, and $In14/In15$ values.

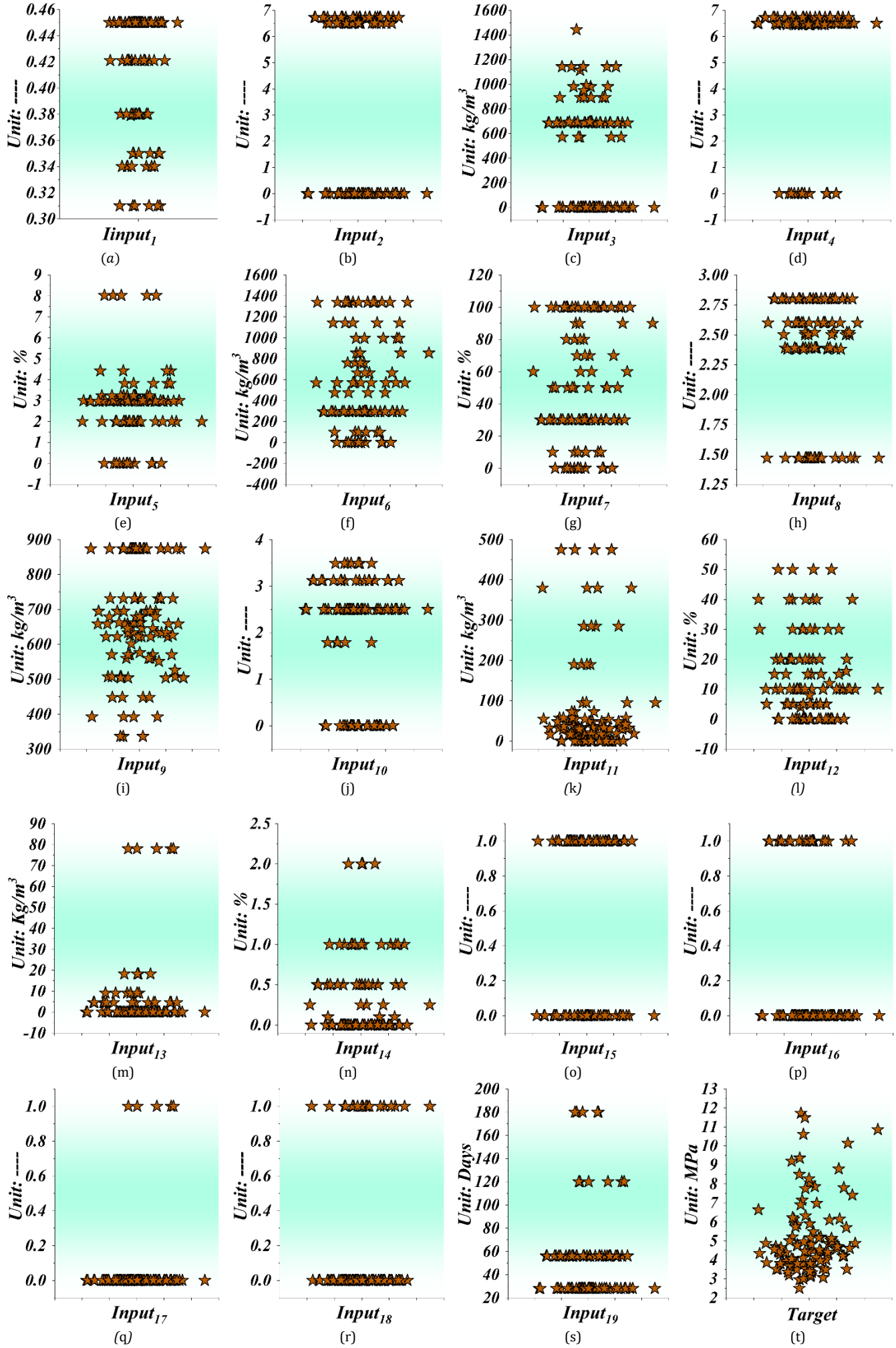

Fig. 1. The distribution of data points

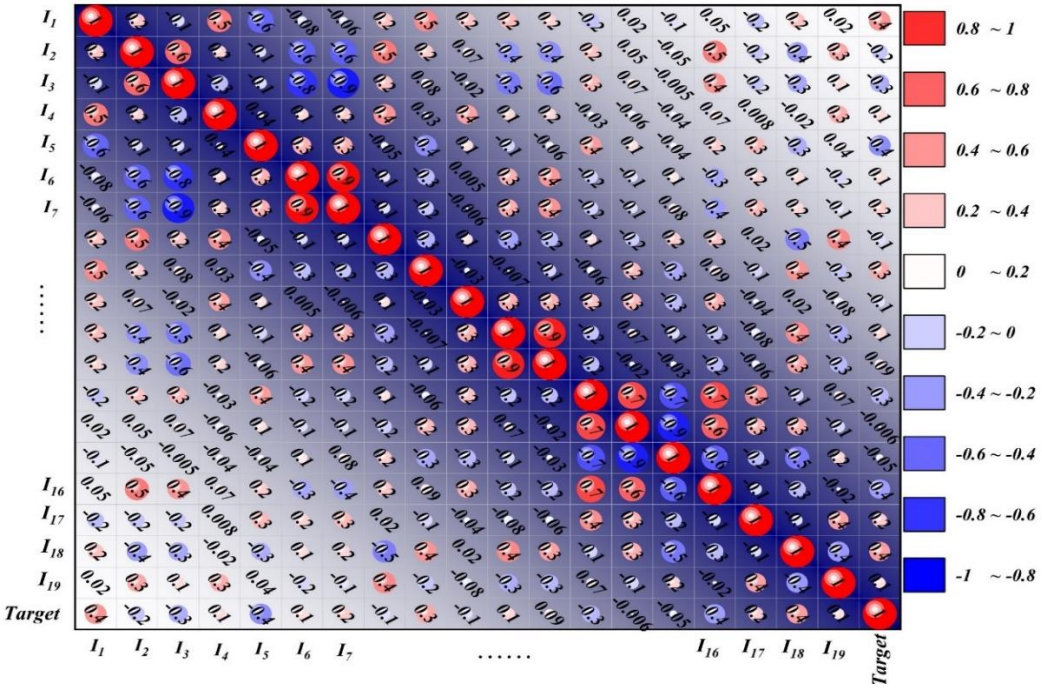

Fig. 2. $Kendall$ correlation values

2.2 Chimp optimization algorithm ($ChOA$)

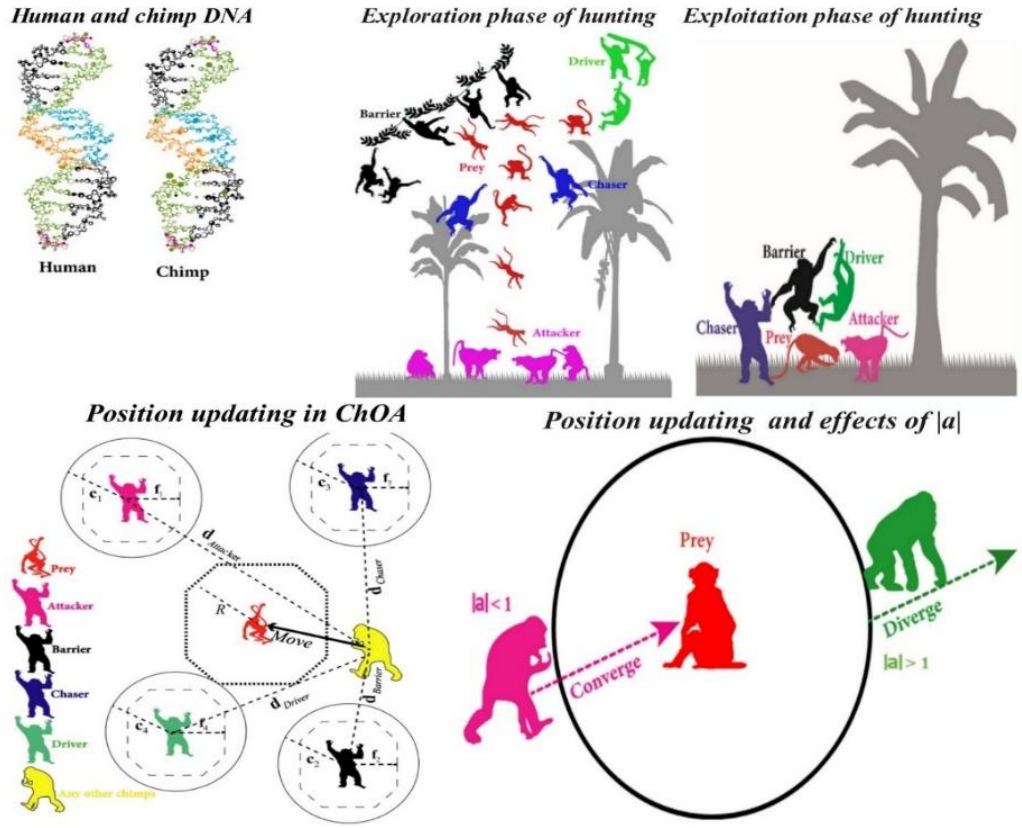

Fig. 3. The overall process of $ChOA$

The $ChOA$ is a strategy based on swarming and impacted by chimpanzees' natural hunting instincts (Liu et al., 2022). The four different categories of agents that make up the community are the driver, chaser, barrier, and attacker. Each chimpanzee in a group has special skills that are necessary for hunting. The underlying mathematical reasons of $ChOA$ are as follows:

$$x_{chimp}^{(t+1)} = x_{prey}^{t} - a \cdot \left| c \cdot x_{prey}^{t} - m \cdot x_{chimp}^{t} \right| \quad (1)$$

In this instance, "x_{prey}^{t}" denotes the prey's place, whereas "x_{chimp}^{t}" denotes the chimpanzees' place. "t" denotes the current iteration, "$\cdot$" denotes the element-wise manufacturing, and the coefficient vectors "a", "m", and "c" are obtained by the application of equations (2) through (4).

$$a = 2 \cdot f \cdot rand_1 - a \quad (2)$$

$$c = 2 \cdot rand_2 \quad (3)$$

$$m = Chaotic\_value \quad (4)$$

The mathematical representations utilized in this research can be discovered in reference (Wang et al., 2011), that defines chaotic diagrams. believe that fifty percent of the chimpanzees will regularly act at the end of this research.

$$x_{chimp}^{(t+1)} = \begin{cases} x_{prey}^{t} - a \cdot d & if \quad \mu < 0.5 \\ Chaotic_{value} & if \quad \mu \geq 0.5 \end{cases} \quad (5)$$

where both ends are included in the uniformly dispersed accidental variable, μ, which ranges from 0 to 1. As a result, random chimpanzees are

used to start $ChOA$. In addition, each individual is placed into one of the four unique groups. Agents then use the classified approach to update the f vector. The four classes then assess the expected locations of their target throughout each repetition. Local minima are successfully eliminated, and the pace of convergence is accelerated by chaotic maps. The figure 3 shows the overall procedure of $ChOA$.

2.3 Artificial rabbit optimization algorithm ($AROA$)

The wild rabbits' defensive tactics are mathematically modeled and integrated into an effective optimization system in the proposed ARA. This approach includes two simulation techniques: random seclusion and detour hunting. In the detour hunting method, the rabbit is encouraged to eat grass near the nests of others, potentially preventing predators from finding its own nest. Additionally, a rabbit can choose to hide randomly in one of its shelters, using a randomized hiding method. This may reduce the chance of being caught by predators. As the rabbits' energy levels decline, they switch from detour hunting to their random hiding strategy [(Wang et al., 2022)

In each iteration, the position of every rabbit in the group is updated according to the algorithm's rules. These new positions are then assessed using the fitness function. As the process continues, the solutions become more accurate. Equation (6) assigns each starting point in the group to a unique location within the search area.

$$Y_i = lb + [ub - lb] \times rand(1, dim) i = 1,2, \dots, n \quad (6)$$

The variable Y_i indicates the animal's position. lb and ub reflect the upper and lower bounds of the variables that is being measured. n and dim denote the sample size and the amount of control factors, respectively.

Detour Foraging

Every individual actively selects a new location adjacent to a randomly selected person from the group, depending on the detour activity of foraging seen in ARA. The numerical explanation for the rabbits' detour hunting is as a result:

$$R_i(it+1) = Y_j(it) + Z \times \left(Y_i(it) - Y_j(it)\right) + rand\left(0.5 \times (0.05 + v_1)\right) \times SND, \quad i,j = 1, \dots, j \neq i \quad (7)$$

$$Z = c \times L \quad (8)$$

$$c(k) = \begin{cases} 1 \; if \; k = g(1) \\ 0 \;\; else \end{cases} \quad k = 1, \dots, dim \; and \; l = 1, \dots, [v_2, dim] \quad (9)$$

$$g = randperm(d), n_1 \sim N(0,1) \quad (10)$$

$$L = sin(2\pi v_3) \times \left(e - e^{((it-1)/T_{max})^2}\right) \quad (11)$$

New and old bunny coordinates are $R_i$and Y_i, respectively, and the standard normally distribution controls SND. The distance traveled, L, reflects velocity. Three random numbers in the [0,1] range are v_1, v_2, and v_3. Iterations max out at T_{max}. round and randperm round to the closest value and randomly permute 1 to dim.

Randomized Hiding

Rabbits often construct many tunnels following their nest as a means of obtaining protection from opponents. A supplementary equation is provided for this purpose.

$$b_{i,j}(it) = Y_i(it) + H.G.Y_i(it), \quad i = 1, \dots, n \; and \; j = 1, \dots, dim \quad (12)$$

$$H = \frac{T_{max} + 1 - it}{T_{max}} \times v_4 \quad (13)$$

$$G(k) = \begin{cases} 1 \; if \; k = j \\ 0 \;\; else \end{cases} \quad k = 1, \dots, dim \quad (14)$$

v_4 is a number that is assigned randomly from a range of 0 to 1. $b_{i,j}$ represents the jth burrow of the ith rabbit. The concealing parameter, denoted as H, gradually grows from 1 to $1/T_{max}$ with a random disturbance applied after each repeat. This characteristic dictates the location where a rabbit will excavate its first underground tunnel, often within close proximity to its immediate surroundings. As the number of iterations increases, the size of this neighborhood decreases.

Rabbits need a secure habitat in order to survive. Consequently, they are reluctant to choose a random hiding spot from a multitude of options in order to avoid being discovered. The random concealment approach may be mathematically represented as follows:

$$R_i(it+1) = Y_i(it) + Z \times \left(v_5 \times b_{i,j}(t) - Y_i(it)\right) \quad i = 1, \dots, n \quad (15)$$

Once either random hiding or detour hunting is effective, the position of the ith rabbit is changed in the next way:

$$Y_i(it+1) = \begin{cases} Y_i(it) & f\left(Y_i(it)\right) \leq f\left(R_i(it+1)\right) \\ R_i(it+1) & f\left(Y_i(it)\right) > f\left(R_i(it+1)\right) \end{cases} \quad (16)$$

Energy Shrink (Switch from Exploration to Exploitation)

That includes an energy component helping one go from the initial step of detour hunting to the latter level of randomized concealment. These justifications relate to the energy factor between this calculation:

$$A(it) = 4\left(1 - \frac{it}{T_{max}}\right) ln\frac{1}{r} \quad (17)$$

The overall procedure of $AROA$ presented in Fig. 4.

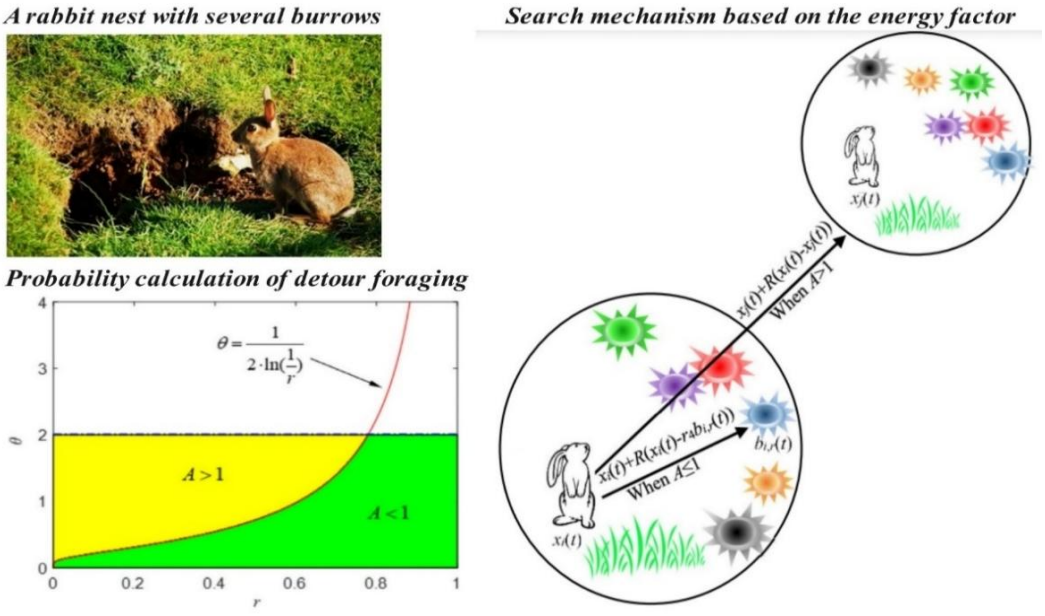

Fig. 4. The overall process of $AROA$

2.4 Least square support vector regression ($LSSVR$) and hybrid forms

In order to develop the Least Squares Support Vector Regression (LSSVR) prediction model for process factors and morphology, the data being used consists of a matrix X derived from the method characteristics (P, V, and F). The outputs, on the other hand, include the aspect ratio, dilution rate, and wetting angle. The $LSSVR$ function $f(x)$ may be represented by equation (18).

$$f_{AR,\eta,\theta}(x) = w^T_{AR,\eta,\theta}\varphi(X) + b_{AR,\eta,\theta} \quad (18)$$

After mapping, $\varphi(X)$ denotes the value of the eigenvector of the variable in the matrix $X = \begin{bmatrix} P_1 & V_2 & F_3 \\ \vdots & \vdots & \vdots \\ P_n & V_n & F_n \end{bmatrix}$, where b acts as the bias term and w denotes the weight coefficient.

The production of the objective function for the $LSSVR$ optimization problem is shown in equation (19). This function is constructed using slack elements and the principle of structural risk minimization.

$$minJ(w,\xi) = \frac{1}{2}w^T w + \frac{1}{2}C\sum_{i=1}^{1}\xi_i^2 \quad (19)$$

The parameter used for regularization is symbolized by the symbol C, while the slack variable is represented by the symbol ξ_i. The $LSSVR$ method converts the SVR discrepancy condition into an equality constraint. Equation (2) demonstrates the necessary condition that must be satisfied for the $LSSVR$ limitation.

$$y_i = w^T\varphi(X) + b + \xi_i \ , i = 1,2,\dots 1 \quad (20)$$

After solving the optimal conditions of the Karush-Kuhn-Tucker (KKT) theorem, the $LSSVR$ prediction function may be obtained as Equation (21). The Lagrange function, given by Equation (22), is inserted to achieve this.

$$f_{AR,\eta,\theta}(x) = \sum_{i=1}^{l} AR,\eta,\theta\ \alpha_i K_{AR,\eta,\theta}(x_i,x) + b_{AR,\eta,\theta} \quad (21)$$

$$L = J(w,\xi) - \sum_{i=1}^{l}\alpha_i\,(w^T\varphi(X) + b + \xi_i - y_i) \quad (22)$$

The sign α_i symbolizes the Lagrange multiplier. The Gaussian kernel function (GKF) is very efficient under general assumptions, potentially reducing computational costs. It is a nonlinear function that utilizes an extra compact support kernel (Wang et al., 2023). It successfully manages the nonlinear relationship between values for parameters and morphology. Hence, according to Equation (23), the GKF is used to augment the sample size for a more accurate alignment with the results obtained in this study.

$$K(x_i,x) = exp\left(-\frac{\|x_i,x_j\|^2}{2\sigma^2}\right) \quad (23)$$

The symbol σ denotes the range of the kernel.

The process of developing an $LSSVR$ simulator starts with the collection of data, followed by training of frameworks, optimisation for hyperparameter assignment, and assessment. These are some of the primary operations that comprise the technique. This is a full list of the stages that are employed to construct designs:

First, the data were cleaned up by eliminating any odd data, filling in any missing values, and deleting any outliers that were found where they were required.

The gathering of data was standardized, and it was split into two sections by way of an appropriate percentage in accordance with the literature: one for learning, and the other for evaluating.

Prior to the beginning of the first $LSSVR$ simulation, the hyperparameters W_{kf} and P_f were assigned starting values that were spaced out within predetermined ranges.

Techniques of optimisation that are considered to be state of the art, including $AROA$ and $ChOA$, were used in order to determine the hyperparameter values that were optimum.

For the purpose of training the $LSSVR$ assessment, a dataset that was specifically collected was utilised.

Following that, it was put through its paces with further datasets selected for evaluating factors, and the hyperparameters that proved to be the most effective were used.

For the purpose of determining whether or not the method is effective, relevant regression metrics are taken into consideration and generated as assessment indicators.

If the results of the assessment indicate that extra hyperparameter tuning is required, then it is performed according to those assessment findings.

The values that have been optimized for the hyperparameters that are associated with $LSSVR$ theories are shown in Table 3, along with the primary values that are for optimisation approaches.

Table 3. The parameters correspond to integrated LSSVRs

Integrated $LSSVR$			
$LSSVR\ and\ ChOA = LSSVR(C)$		$LSSVR\ and\ AROA = LSSVR(A)$	
Properties	Value	Properties	Value
Number of iterations	300	Number of iterations	300
Total number of runs	5	Total number of runs	5
Population number	20	Population number	15
r_1 and r_2	[0,1]	Parameter free	–
m	Chaotic		
Kernel width	188.96	Kernel width	225.8
Penalty factor	1.13	Penalty factor	0.952

2.5 Workability metrics

Indicators are often used in machine learning and statistics to assess how well models perform, especially when regression analysis is involved. The precision and dependability of the $LSSVR(C)$ and $LSSVR(A)$s was compared in this research using the following eight criteria. When comparing these measures, the model's precision and correlation are greater when the R^2, and $A_{10.index}$ number is higher. On the other hand, the error-based measures with lesser values—PI, $U_{95\%}$, SI, $RMSE$, MAE, and $SMAPE$—are valuable. In addition to this, a 95% confidence level was used to complete the analysis of uncertainty (the lower one is excellent).

Performance index:

$$PI = \frac{1}{\bar{X}}\frac{RMSE}{\sqrt{R^2+1}} \quad (24)$$

A_{10} index:

$$A_{10} = \frac{g_{10}}{G} \quad (25)$$

Uncertainty analysis with a 95% confidence level:

$$U_{95} = 1.96\sqrt{(SD^2 + RMSE^2)} \quad (26)$$

Scatter index:

$$SI = \frac{\sqrt{\left(\frac{1}{D}\right)\sum_{g=1}^{D}\left(\left(X_g - \bar{X}\right) - \left(Y_g - \bar{Y}\right)\right)^2}}{\left(\frac{1}{D}\right)\sum_{g=1}^{D} Y_g} \quad (27)$$

Coefficient of determination:

$$R^2 = \left(\frac{\sum_{g=1}^{D}(X_i - \bar{X})(Y_g - \bar{Y})}{\sqrt{\left[\sum_{g=1}^{D}(X_i - X)^2\right]\left[\sum_{g=1}^{D}\left(Y_g - \bar{Y}\right)^2\right]}}\right) \quad (28)$$

Mean square error:

$$RMSE = \sqrt{\frac{1}{D}\sum_{g=1}^{D}\left(Y_g - X_g\right)^2} \quad (29)$$

Mean absolute error:

$$MAE = \frac{1}{D}\sum_{g=1}^{D}\left|Y_i - X_g\right| \quad (30)$$

Symmetric Mean Absolute Percentage Error:

$$SMAPE = \frac{1}{D}\sum_{g=1}^{D}\frac{\left|X_g - Y_g\right|}{\frac{\left(\left|X_g\right| + \left|Y_g\right|\right)}{2}} \times 100 \quad (31)$$

The computations that were done produced the following result: The numbers presented are the average of the expected quantity ($\bar{Y}$), the expected value (Y_g), and the total number of observations (D). On the other hand, $\bar{X}$ represents the average value of the observed f_s, while X_g represents observed f_s.

3. Results

It is possible to discover the f_s of $FRRAC$ by combining the $LSSVR$ approach with the $AROA$ and $ChOA$ techniques, which are also referred to as $LSSVR(C)$ and $LSSVR(A)$ combinations. Fig 5 illustrates both the expected and measured f_s for the $LSSVR(C)$ and $LSSVR(A)$ techniques throughout the training and assessment phases of the process. Additionally, the graphic illustrates the comparison between the predicted f_s ratio and the measured f_s ratio. In order to evaluate the precision of the methods in forecasting f_s, a number of measures were utilized. These metrics included PI, $A_{10.index}$, $U_{95\%}$, SI, R^2, $RMSE$, MAE, and $SMAPE$ which were utilized. Both the evaluations of the product development strategy and the assessments of the designs that were developed during the learning procedure are included in Table 3, which presents the data from both analyses. In the present research, a score was awarded to each model for each measure at each stage of the computation procedure. This was done with the intention of improving the accuracy of the integrated models. In addition, the research intends to evaluate the precision and reliability of the predictions that were developed by contrasting its findings with those of previous research which was conducted on XGB and RF (Alkayem et al., 2024).

Both the $LSSVR(A)$ and $LSSVR(C)$ approaches provide a significant amount of promise for precise f_s prediction, as indicated by the presented findings. Throughout the training and evaluation process, the $LSSVR(A)$ technique demonstrated exceptional dependability with R^2 values of 0.9895 and 0.9825. R^2 values of 0.982 and 0.968, accordingly, indicate that the results for $LSSVR(A)$ were much bigger than those for $LSSVR(C)$. $A_{10.index}$, the most accurate model representations, are expected metrics with a comparable performance trend, with the exception of the training period. When it comes to these measures, the models perform quite similarly when tested, while $LSSVR(A)$ performs much better during training. It is useful to assess the dependability of the method utilising additional error-based measures. Remember that for certain performance

measurements, lower values imply higher efficiency. Throughout the training and assessment stages, the $LSSVR(A)$ generated the lowest $SMAPE$ index values, measuring 2.9206 and 3.201, accordingly. In comparison with the numbers that $LSSVR(C)$ obtained throughout the assessment and learning stages, which were 3.2281 and 4.9232, respectively, these results demonstrated a higher degree of accuracy. As can be shown, the $LSSVR(A)$ has the capacity to forecast competency and reliability. The difference percentages between the two models developed for these measures are at least 4%; in some cases, the gap is reduced by 47%.

Table 4. The results corresponding to integrated LSSVRs

Metrics	$LSSVR(C)$	Rank score	$LSSVR(A)$	Rank score	Variance (%)	XGB (Alkayem et al., 2024)	RF (Alkayem et al., 2024)
			Train section				
PI	0.0258	1	0.0199*	2	-22.8682		
$A_{10.index}$	0.974	2	0.961	1	-1.3347		
$U_{95\%}$	0.7411	1	0.5741	2	-22.5341		
SI	0.0514	1	0.0397	2	-22.7626		
R^2	0.982	1	0.9895	2	0.76375	0.9979	0.9845
$RMSE$	0.2671	1	0.2064	2	-22.7256	0.0882	0.2411
MAE	0.1685	1	0.1414	2	-16.0831	0.0432	0.1732
$SMAPE$	3.2281	1	2.9206	2	-9.52573		
			Test section				
PI	0.0691	1	0.036	2	-47.9016		
$A_{10.index}$	0.92	1	0.96	2	4.34783		
$U_{95\%}$	1.9088	1	1.0121	2	-46.9772		
SI	0.1349	1	0.0717	2	-46.8495		
R^2	0.968	1	0.9825	2	1.49793	0.7684	0.8964
$RMSE$	0.6893	1	0.3664	2	-46.8446	0.9617	0.6431
MAE	0.2991	1	0.1909	2	-36.1752	0.5001	0.4012
$SMAPE$	4.9232	1	3.201	2	-34.9813		
Total ranking score		17		31			

* Bold values are the best value

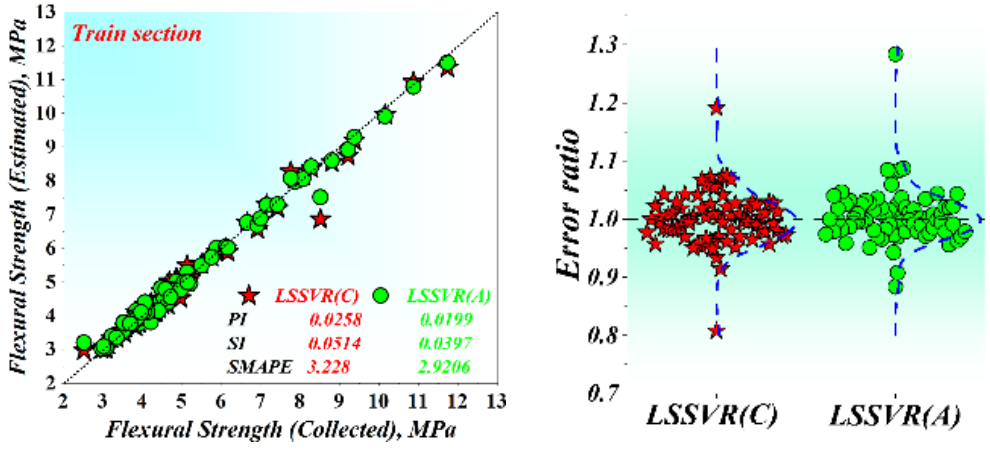

(a) Train section

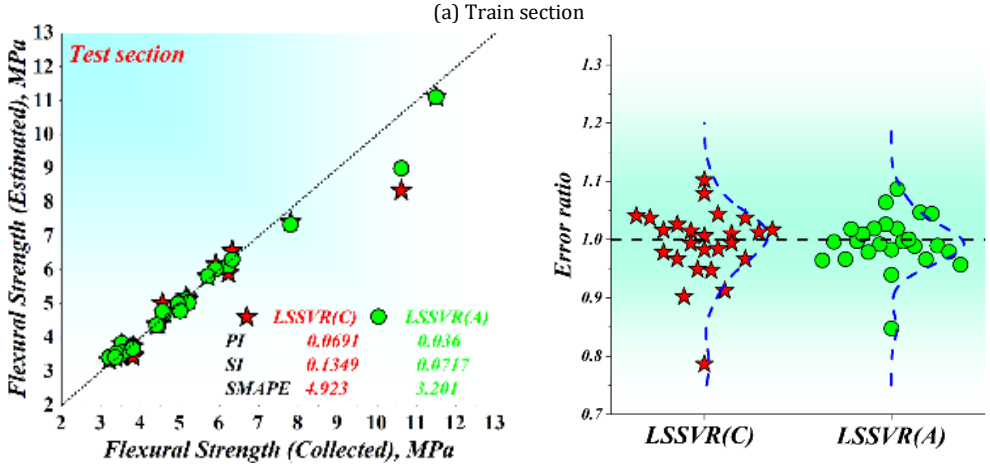

(b) Test section

Fig. 5. The results corresponding to integrated LSSVRs

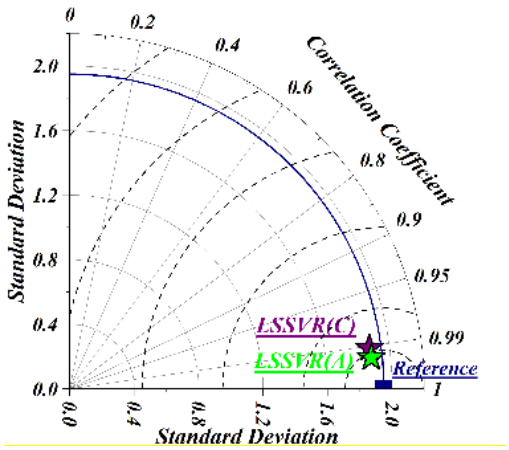

(a) Train section

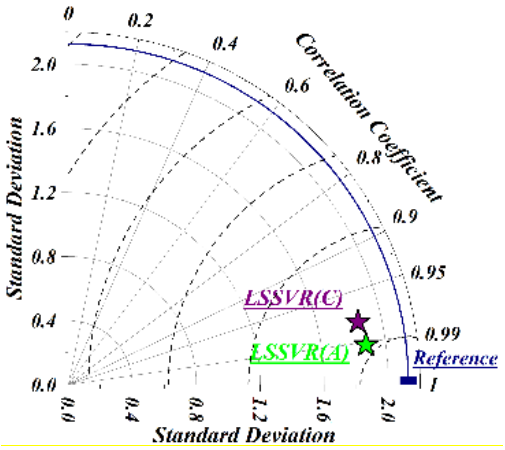

(b) Test section

Fig. 6. The Taylor Diagram analysis on the developed models

The idea of measuring uncertainty at a 95% confidence level, or U_{95}, is used in this study to suggest that there is a 95% chance that the measured value will fall within the range around the observed or anticipated value. By taking into account both measurement variation and forecast accuracy, $U95$ provides an accurate estimate of uncertainty. This makes the level of reliance more transparent, which helps with decision-making. The $LSSVR(A)$ had the lowest U_{95} index values, measuring 0.5741 and 1.0121, accordingly, during the learning and evaluation phases. But during the training and evaluation phases, the values obtained by $LSSVR(C)$, that were 0.7411 and 1.9088, were greater than these values. These settings persisted over the whole process. It has been demonstrated through logical inference and evaluation standards that both models are valid and dependable, with $LSSVR(A)$ showing a little advantage over the other model.

In Fig 5, we have an illustration of the ratio of the observed f_s to the anticipated f_s, that is tracked during the learning and evaluation phases. This ratio incorporates the conventional Lorentz distribution as a component into its own calculation. Below the main figure, we provide a more compact distribution that has a noticeable peak and upper and lower limits that are tightly limited. This allows us to evaluate the robustness of the model. The results unambiguously reveal that the $LSSVR(A)$ model is superior to the $LSSVR(C)$ model in each and every phase of the process. This is presented by boundaries that have good definition and a peak that is more prominent, particularly when the ratio is 1.

By doing a comprehensive comparing with the previous study, that covers models like XGB and RF, the models' reliability is shown (Alkayem et al., 2024).

Comparison of performance and robustness (see Table 4). The proposed LSSVR(A) surpasses previous studies when evaluated with similar metrics (R^2, MAE, RMSE) and is more accurate and consistent than both XGB and RF [42]. LSSVR(A) records higher R^2 and lower MAE/RMSE during both training and testing phases, demonstrating better generalization rather than phase-specific optimization. Specifically, MAE drops relative to RF by 18.36% in training (0.1732 to 0.1414) and by 52.42% in testing (0.4012 to 0.1909). Compared to XGB, the testing MAE improves by 61.83% (0.5001 to 0.1909). Notably, XGB's very small training MAE (0.0432) contrasted with its much larger testing MAE (0.5001) indicates overfitting; conversely, LSSVR(A)'s balanced training and testing errors (0.1414/0.1909) contribute to better generalization and operational reliability. Practically, these improvements lead to narrower prediction intervals for FRRAC flexural strength, allowing for leaner mix designs and more confident QA/QC decisions with fewer re-tests, while maintaining safety margins.

The Taylor Diagram in Fig. 6 provides a comparative visualization of the performance of the two hybrid models (LSSVR(A) and LSSVR(C)) in both the training and testing phases. In both sections, the LSSVR(A) model is positioned closer to the reference point, indicating a higher correlation coefficient, lower standard deviation difference, and better overall agreement with the experimental data. Conversely, the LSSVR(C) model shows slightly larger deviations, reflecting relatively lower accuracy and higher prediction uncertainty. This comparison confirms that LSSVR(A) exhibits superior predictive performance and stability in modeling the flexural strength of FRRAC.

Regarding the developed study, some limitations and the most related suggestions could be recognized as follows. The 102 samples that make up the study's small dataset might restrict how far the findings can be applied. Therefore, increase the dataset's size by gathering additional samples from various resources to boost the dependability and robustness of the model. When paired with methodologies such as $ChOA$ and $AROA$, the $LSSVR$ model may be computationally demanding, which presents issues for scalability and real-time applications. To fix this and make the model more useful for real-world applications, investigate ways to maximise computational efficiency, such as more effective computing approaches or streamlined methods. The research concentrates on certain kinds of recycled materials (RCA and CR) with defined qualities; hence, variations in the composition and quality of these materials frcom other resources might impact the precision of the model. To further improve the model's comprehensiveness and flexibility, include a greater variety of input parameters, such as additives, ambient conditions, and fibre kinds. The lack of external datasets from various geographic regions or climatic conditions to evaluate the models may have compromised the applicability of the results. Additionally, to assess the models' precision and practical applicability, conduct real-world testing and validate them utilizing external datasets from diverse places and situations. Through empirical research and long-term monitoring, examine the long-term performance and stability of $FRRAC$ as anticipated by these models. To promote sustainable practices, carry out a thorough study of the environmental effect. Enhancing the predictive modelling of flexural strength in $FRRAC$ may lead to more sustainable and effective building methods by resolving these constraints and putting the relevant suggestions into practice.

Turning to the practical applications, the predictive models enable engineers to create $FRRAC$ mixes with the appropriate flexural strength, guaranteeing that the finished concrete satisfies certain structural specifications. Customized concrete formulas that strike a balance between performance, affordability, and sustainability are made possible by this. Also, before concrete is utilized in structural applications, construction firms may use these models to estimate and confirm the material's flexural strength as part of their quality control procedures. Moreover, by ensuring that only concrete with sufficient strength is used, structures and infrastructure will be safer and more resilient. The building industry may save waste and lessen its need on natural aggregates by adding recycled materials like RCA and CR to concrete. Interestingly, the use of predictive models guarantees that the structural integrity of the concrete is not jeopardised by the use of sustainable materials. By experimenting with various ratios of recycled materials and additions, researchers may quickly design new, more environmentally friendly concrete compositions by using these models. Furthermore, the models may be utilized to evaluate and forecast how well $FRRAC$ will work in the rehabilitation of already-existing buildings, especially when it comes to fixing or strengthening ageing infrastructure. These models provide useful insights into the application of machine learning in building material science, making them useful teaching aids for students studying civil engineering. These results have direct engineering implications for FRRAC beyond numerical advantages. Lower prediction errors enhance mix design by reducing overdesign, saving materials, and lowering embodied carbon while maintaining reliability. They enable more precise safety margins, support better partial factor decisions, and avoid under- or overestimation. Improved accuracy reduces lab iterations, shortens development cycles, cuts testing costs, and helps acceptance tests with fewer re-tests. Better strength predictions optimize fiber dosage, meeting performance needs without extra costs or workability issues. For asset management, sharper flexural capacity estimates prioritize interventions and justify approvals. To ensure comparability, we retain PI and other indices and will include MAPE in future work for comprehensive assessment.

In the Discussion, we also examine the study's limitations and suggest directions for future research, summarized below.

This study is limited by a small dataset of 102 samples used for model development, which may restrict its broader applicability and increase the risk of overfitting, despite using a 75%/25% train–test split and reporting uncertainty at a 95% confidence level. To improve robustness and

external validity, future research should expand the dataset with samples from diverse sources and test the models against external data from different geographic and climatic conditions. Additionally, combining LSSVR with metaheuristic optimizers (AROA/ChOA) can be computationally intensive, challenging scalability and real-time application; thus, enhancing computational efficiency through streamlined solvers or more effective approaches is advisable. Finally, since the study targets specific recycled constituents with certain properties, variations in composition and quality of other recycled aggregates and rubber sources may influence accuracy. Incorporating a broader range of input features (such as additives, ambient conditions, fiber types) and conducting real-world and long-term testing is recommended to increase the models' generalizability, stability, and practical utility.

4. Main remarks

For the purpose of determining and evaluating the most efficient regression-based and machine learning strategies for forecasting flexural strength (f_s) in fiber-reinforced rubberized recycled aggregate concrete ($FRRAC$), the purpose of this study is to discover and evaluate the most effective methodologies. Through the use of a computer software called Least square support vector regression ($LSSVR$) analysis, that utilises a method that is based on regression, this objective was successfully accomplished. In this work, the $LSSVR$ analysis was used in conjunction with two methods of metaheuristic optimisation, notably the Artificial rabbit optimisation algorithm ($AROA$) and the Chimp optimisation algorithm ($ChOA$). The purpose of these procedures was to discover the appropriate values for the deciding variables.

The Kendall coefficients for RCA quantity ($In6$)/RCA substitution level ($In7$) and CR replacement level ($In12$)/CR amount ($In11$) are 0.9, indicating a significant positive correlation. The Kendall coefficient, -0.9, shows the strongest negative correlation between NCA quantity ($In3$)/RCA substitution level ($In7$) and Fibre amount ($In14$)/Kind of fibre (No fibre) ($In15$).

According to the results, $LSSVR(A)$ and $LSSVR(C)$ provide promising f_s prediction. During training and assessment, the $LSSVR(A)$ approach showed high reliability with R^2 values of 0.9895 and 0.9825. R^2 values of 0.982 and 0.968 suggest that $LSSVR(A)$ yielded significantly higher outcomes than $LSSVR(C)$. $A_{10.index}$, the highest precise model representations, predicts a similar performance pattern except for training.

The $LSSVR(A)$ had the lowest $SMAPE$ index values throughout training and evaluation, 2.9206 and 3.201. These findings were more accurate than $LSSVR(C)$'s 3.2281 and 4.9232 during evaluation and learning. As proven, $LSSVR(A)$ predicts competence and dependability. The two models that were created for these measurements have different percentages of at least 4%; in some circumstances, the difference is as little as 47%.

Throughout training and assessment, the $LSSVR(A)$ had the lowest U_{95} index values (0.5741 and 1.0121), indicating trustworthiness and decision-making. However, $LSSVR(C)$ values of 0.7411 and 1.9088 were higher throughout training and assessment.

Compared to XGB and RF [Literature], this investigation is more precise and robust. The higher R^2 values and lower MAE and $RMSE$ values demonstrate this. Training and assessment improvements were found for XGB and RF models. In the learning stage, the XGB model outperforms R^2, $RMSE$, and MAE computations in dependability. The MAE reduced from 0.1732 in RF to 0.1414 in $LSSVR(A)$ during training. During assessment, MAE reduced from 0.4012 in RF to 0.1909 in $LSSVR(A)$. The MAE changed from 0.5001 in XGB to 0.1909 in $LSSVR(A)$ during assessment. It also increased from 0.0432 in XGB to 0.1414 in $LSSVR(A)$ during learning.

Turning to the practical applications, the predictive models enable engineers to create $FRRAC$ mixes with the appropriate flexural strength, guaranteeing that the finished concrete satisfies certain structural specifications. Customized concrete formulas that strike a balance between performance, affordability, and sustainability are made possible by this. Moreover, by ensuring that only concrete with sufficient strength is used, structures and infrastructure will be safer and more resilient. The building industry may save waste and lessen its need on natural aggregates by adding recycled materials like RCA and CR to concrete. Interestingly, the use of predictive models guarantees that the structural integrity of the concrete is not jeopardized by the use of sustainable materials.

Competing of interests

The authors declare no competing of interests.

Authorship Contribution Statement

Yuexiang Li: Writing-Original draft preparation, Conceptualization, Supervision, Project administration.

Liqing Hao: Methodology, Software

Dongfang Zhang: Validation.

References

Ahmed, H., Tiznobaik, M., Alam, M.S., 2019. Mechanical and durability properties of rubberized recycled aggregate concrete, in: CSCE Annual Conference: Canada.

Alabduljabbar, H., Farooq, F., Alyami, M., Hammad, A.W.A., 2024. Assessment of the split tensile strength of fiber reinforced recycled aggregate concrete using interpretable approaches with graphical user interface. Mater Today Commun 38, 108009. https://doi.org/10.1016/j.mtcomm.2023.108009

Alarfaj, M., Qureshi, H.J., Shahab, M.Z., Javed, M.F., Arifuzzaman, M., Gamil, Y., 2024. Machine learning based prediction models for spilt tensile strength of fiber reinforced recycled aggregate concrete. Case Studies in Construction Materials 20, e02836. https://doi.org/10.1016/j.cscm.2023.e02836

Alkayem, N.F., Shen, L., Mayya, A., Asteris, P.G., Fu, R., Di Luzio, G., Strauss, A., Cao, M., 2024. Prediction of concrete and FRC properties at high temperature using machine and deep learning: a review of recent advances and future perspectives. Journal of Building Engineering 83, 108369. https://doi.org/10.1016/j.jobe.2023.108369

Aslani, F., Ma, G., Wan, D.L.Y., Muselin, G., 2018. Development of high-performance self-compacting concrete using waste recycled concrete aggregates and rubber granules. J Clean Prod 182, 553–566. https://doi.org/10.1016/j.jclepro.2018.02.074

Bahraq, A.A., Jose, J., Shameem, M., Maslehuddin, M., 2022. A review on treatment techniques to improve the durability of recycled aggregate concrete: Enhancement mechanisms, performance and cost analysis. Journal of Building Engineering 55, 104713. https://doi.org/10.1016/j.jobe.2022.104713

Bandarage, K., Sadeghian, P., 2020. Effects of long shredded rubber particles recycled from waste tires on mechanical properties of concrete. J Sustain Cem Based Mater 9, 50–59. https://doi.org/10.1080/21650373.2019.1676839

Cakiroglu, C., Shahjalal, M., Islam, K., Mahmood, S.M.F., Billah, A.H.M.M., Nehdi, M.L., 2023. Explainable ensemble learning data-driven modeling of mechanical properties of fiber-reinforced rubberized recycled aggregate concrete. Journal of Building Engineering 76, 107279. https://doi.org/10.1016/j.jobe.2023.107279

Chen, M., Mangalathu, S., Jeon, J.-S., 2022. Machine learning–based seismic reliability assessment of bridge networks. Journal of Structural Engineering 148, 06022002. https://doi.org/10.1061/(ASCE)ST.1943-541X.0003376

Çiftçioğlu, A.Ö., Delikanlı, A., Shafighfard, T., Bagherzadeh, F., 2025. Machine learning based shear strength prediction in reinforced concrete beams using Levy flight enhanced decision trees. Sci Rep 15, 27488. https://doi.org/10.1038/s41598-025-12359-y

de-Prado-Gil, J., Palencia, C., Jagadesh, P., Martínez-García, R., 2022. A comparison of machine learning tools that model the splitting tensile strength of self-compacting recycled aggregate concrete. Materials 15, 4164. https://doi.org/10.3390/ma15124164

El-Khoja, A.M.N., Ashour, A.F., Abdalhmid, J., Dai, X., Khan, A., 2018. Prediction of rubberised concrete strength by using artificial neural networks. training 30, 35.

Espinosa, A.B., Revilla-Cuesta, V., Skaf, M., Faleschini, F., Ortega-López, V., 2023. Utility of ultrasonic pulse velocity for estimating the overall mechanical behavior of recycled aggregate self-compacting concrete. Applied Sciences 13, 874. https://doi.org/10.3390/app13020874

Golafshani, E.M., Arashpour, M., Kashani, A., 2021. Green mix design of rubbercrete using machine learning-based ensemble model and constrained multi-objective optimization. J Clean Prod 327, 129518. https://doi.org/10.1016/j.jclepro.2021.129518

Grammelis, P., Margaritis, N., Dallas, P., Rakopoulos, D., Mavrias, G., 2021. A review on management of end-of-life tires (ELTs) and alternative uses of textile fibers. Energies (Basel) 14, 571. https://doi.org/10.3390/en14030571

Guo, Y., Zhang, J., Chen, G., Xie, Z., 2014. Compressive behaviour of concrete structures incorporating recycled concrete aggregates, rubber crumb and reinforced with steel fibre, subjected to elevated temperatures. J Clean Prod 72, 193–203. https://doi.org/10.1016/j.jclepro.2014.02.036

Gupta, T., Patel, K.A., Siddique, S., Sharma, R.K., Chaudhary, S., 2019. Prediction of mechanical properties of rubberised concrete exposed to elevated temperature using ANN. Measurement 147, 106870. https://doi.org/10.1016/j.measurement.2019.106870

Hemmatian, A., Jalali, M., Naderpour, H., Nehdi, M.L., 2023. Machine learning prediction of fiber pull-out and bond-slip in fiber-reinforced cementitious composites. Journal of Building Engineering 63, 105474. https://doi.org/10.1016/j.jobe.2022.105474

Henry, M., Yamashita, H., Nishimura, T., Kato, Y., 2012. Properties and mechanical–environmental efficiency of concrete combining recycled rubber with waste materials. International Journal of Sustainable Engineering 5, 66–75. https://doi.org/10.1080/19397038.2011.569584

Hossain, F.M.Z., Shahjalal, M., Islam, K., Tiznobaik, M., Alam, M.S., 2019. Mechanical properties of recycled aggregate concrete containing crumb rubber and polypropylene fiber. Constr Build Mater 225, 983–996. https://doi.org/10.1016/j.conbuildmat.2019.07.245

Huang, X., Zhang, J., Sresakoolchai, J., Kaewunruen, S., 2021. Machine learning aided design and prediction of environmentally friendly rubberised concrete. Sustainability 13, 1691. https://doi.org/10.3390/su13041691

Islam, M.J., Shahjalal, M., 2021. Effect of polypropylene plastic on concrete properties as a partial replacement of stone and brick aggregate. Case Studies in Construction Materials 15, e00627. https://doi.org/10.1016/j.cscm.2021.e00627

Kazemi, F., Çiftçioğlu, A. Özyüksel, Shafighfard, T., Asgarkhani, N., Jankowski, R., 2025. RAGN-R: A multi-subject ensemble machine-learning method for estimating mechanical properties of advanced structural materials. Comput Struct 308, 107657. https://doi.org/10.1016/j.compstruc.2025.107657

Kazemi, F., Shafighfard, T., Yoo, D.-Y., 2024. Data-driven modeling of mechanical properties of fiber-reinforced concrete: a critical review. Archives of Computational Methods in Engineering 31, 2049–2078. https://doi.org/10.1007/s11831-023-10043-w

Li, L.-J., Tu, G.-R., Lan, C., Liu, F., 2016. Mechanical characterization of waste-rubber-modified recycled-aggregate concrete. J Clean Prod 124, 325–338. https://doi.org/10.1016/j.jclepro.2016.03.003

Liu, F., Meng, L., Ning, G.-F., Li, L.-J., 2015. Fatigue performance of rubber-modified recycled aggregate concrete (RRAC) for pavement. Constr Build Mater 95, 207–217. https://doi.org/10.1016/j.conbuildmat.2015.07.042

Liu, L., Khishe, M., Mohammadi, M., Mohammed, A.H., 2022. Optimization of constraint engineering problems using robust universal learning chimp optimization. Advanced Engineering Informatics 53, 101636. https://doi.org/10.1016/j.aei.2022.101636

Marie, I., 2017. Thermal conductivity of hybrid recycled aggregate–Rubberized concrete. Constr Build Mater 133, 516–524. https://doi.org/10.1016/j.conbuildmat.2016.12.113

Mhaya, A.M., Huseien, G.F., Abidin, A.R.Z., Ismail, M., 2020. Long-term mechanical and durable properties of waste tires rubber crumbs replaced GBFS modified concretes. Constr Build Mater 256, 119505. https://doi.org/10.1016/j.conbuildmat.2020.119505

Miladirad, K., Golafshani, E.M., Safehian, M., Sarkar, A., 2021. Modeling the mechanical properties of rubberized concrete using machine learning methods. Computers and Concrete 28, 567–583. https://doi.org/10.12989/cac.2021.28.6.567

Moustafa, A., ElGawady, M.A., 2017. Dynamic properties of high strength rubberized concrete. ACI Spec. Publ 314, 1–22.

Pal, A., Ahmed, K.S., Hossain, F.M.Z., Alam, M.S., 2023. Machine learning models for predicting compressive strength of fiber-reinforced concrete containing waste rubber and recycled aggregate. J Clean Prod 423, 138673. https://doi.org/10.1016/j.jclepro.2023.138673

Pal, A., Ahmed, K.S., Mangalathu, S., 2024. Data-driven machine learning approaches for predicting slump of fiber-reinforced concrete containing waste rubber and recycled aggregate. Constr Build Mater 417, 135369. https://doi.org/10.1016/j.conbuildmat.2024.135369

Piri, M., Shirzadi Javid, A.A., Momen, R., 2023. Investigation of mechanical and durability properties of recycled aggregate concrete containing crumb rubber considering a new model of elastic modulus. Scientia Iranica. https://doi.org/10.24200/sci.2023.60833.7013

Qaidi, S.M.A., Dinkha, Y.Z., Haido, J.H., Ali, M.H., Tayeh, B.A., 2021. Engineering properties of sustainable green concrete incorporating eco-friendly aggregate of crumb rubber: A review. J Clean Prod 324, 129251. https://doi.org/10.1016/j.jclepro.2021.129251

Rahman, J., Ahmed, K.S., Khan, N.I., Islam, K., Mangalathu, S., 2021. Data-driven shear strength prediction of steel fiber reinforced concrete beams using machine learning approach. Eng Struct 233, 111743. https://doi.org/10.1016/j.engstruct.2020.111743

Revilla-Cuesta, V., Ortega-López, V., Faleschini, F., Espinosa, A.B., Serrano-López, R., 2022a. Hammer rebound index as an overall-mechanical-quality indicator of self-compacting concrete containing recycled concrete aggregate. Constr Build Mater 347, 128549. https://doi.org/10.1016/j.conbuildmat.2022.128549

Revilla-Cuesta, V., Shi, J., Skaf, M., Ortega-López, V., Manso, J.M., 2022b. Non-destructive density-corrected estimation of the elastic modulus of slag-cement self-compacting concrete containing recycled aggregate. Developments in the Built Environment 12, 100097. https://doi.org/10.1016/j.dibe.2022.100097

Shafighfard, T., Asgarkhani, N., Kazemi, F., Yoo, D.-Y., 2025. Transfer learning on stacked machine-learning model for predicting pull-out behavior of steel fibers from concrete. Eng Appl Artif Intell 158, 111533. https://doi.org/10.1016/j.engappai.2025.111533

Shafighfard, T., Bagherzadeh, F., Rizi, R.A., Yoo, D.-Y., 2022. Data-driven compressive strength prediction of steel fiber reinforced concrete (SFRC) subjected to elevated temperatures using stacked machine learning algorithms. Journal of Materials Research and Technology 21, 3777–3794. https://doi.org/10.1016/j.jmrt.2022.10.153

Shahjalal, M., 2022. Compressive and free vibration response of fiber reinforced rubberized recycled concrete columns. http://lib.buet.ac.bd:8080/xmlui/handle/123456789/6262

Shahjalal, M., Hossain, F.M.Z., Islam, K., Tiznobaik, M., Alam, M.S., 2019. Experimental study on the mechanical properties of recycled aggregate concrete using crumb rubber and polypropylene fiber, in: CSCE Annual Conference, Canada.

Su, H., 2015. Properties of concrete with recycled aggregates as coarse aggregate and as-received/surface-modified rubber particles as fine aggregate. https://etheses.bham.ac.uk/id/eprint/6003/

Wang, C., Ling, Y., Wang, L., Yang, B., Shi, W., 2025. A Carbon Sequestered Superhydrophobic Mortar with Enhanced Anti-chloride Ions Penetration and Frost Resistance. Cem Concr Compos 106167. https://doi.org/10.1016/j.cemconcomp.2025.106167

Wang, H., Wu, Z., Rahnamayan, S., Liu, Y., Ventresca, M., 2011. Enhancing particle swarm optimization using generalized opposition-based learning. Inf Sci (N Y) 181, 4699–4714. https://doi.org/10.1016/j.ins.2011.03.016

Wang, J., Lin, T., Ma, S., Ju, J., Wang, R., Chen, G., Jiang, R., Wang, Z., 2023. The qualitative and quantitative analysis of industrial paraffin contamination levels in rice using spectral pretreatment combined with machine learning models. Journal of Food Composition and Analysis 121, 105430. https://doi.org/10.1016/j.jfca.2023.105430

Wang, L., Cao, Q., Zhang, Z., Mirjalili, S., Zhao, W., 2022. Artificial rabbits optimization: A new bio-inspired meta-heuristic algorithm for solving engineering optimization problems. Eng Appl Artif Intell 114, 105082. https://doi.org/10.1016/j.engappai.2022.105082

Xie, J., Fang, C., Lu, Z., Li, Z., Li, L., 2018. Effects of the addition of silica fume and rubber particles on the compressive behaviour of recycled aggregate concrete with steel fibres. J Clean Prod 197, 656–667. https://doi.org/10.1016/j.jclepro.2018.06.237

Xie, J., Guo, Y., Liu, L., Xie, Z., 2015. Compressive and flexural behaviours of a new steel-fibre-reinforced recycled aggregate concrete with crumb rubber. Constr Build Mater 79, 263–272. https://doi.org/10.1016/j.conbuildmat.2015.01.036

Zhang, J., Xu, J., Liu, C., Zheng, J., 2021. Prediction of rubber fiber concrete strength using extreme learning machine. Front Mater 7, 582635. https://doi.org/10.3389/fmats.2020.582635

Zhang, P., Wang, C., Guo, J., Wu, J., Zhang, C., 2024. Production of sustainable steel fiber-reinforced rubberized concrete with enhanced mechanical properties: A state-of-the-art review. Journal of Building Engineering 109735. https://doi.org/10.1016/j.jobe.2024.109735

Zhang, P., Wang, W., Guo, J., Zheng, Y., 2025. Abrasion resistance and damage mechanism of hybrid fiber-reinforced geopolymer concrete containing nano-SiO2. J Clean Prod 494, 144971. https://doi.org/10.1016/j.jclepro.2025.144971

Disclaimer